

Variable Accretion Outbursts in Protostellar Evolution

Jaehan Bae¹, Lee Hartmann¹, Zhaohuan Zhu², Charles Gammie^{3,4}

jaehbae@umich.edu, lhartm@umich.edu, zhuzh@astro.princeton.edu,
gammie@illinois.edu

ABSTRACT

We extend the one-dimensional, two-zone models of long-term protostellar disk evolution with infall of Zhu et al. to consider the potential effects of a finite viscosity in regions where the ionization is too low for the magnetorotational instability (MRI) to operate (the “dead zone”). We find that the presence of a small but finite dead zone viscosity, as suggested by simulations of stratified disks with MRI-active outer layers, can trigger inside-out bursts of accretion, starting at or near the inner edge of the disk, instead of the previously-found outside-in bursts with zero dead zone viscosity, which originate at a few AU in radius. These inside-out bursts of accretion bear a qualitative resemblance to the outburst behavior of one FU Ori object, V1515 Cyg, in contrast to the outside-in burst models which more closely resemble the accretion events in FU Ori and V1057 Cyg. Our results suggest that the type and frequency of outbursts are potentially a probe of transport efficiency in the dead zone. Simulations must treat the inner disk regions, $R \lesssim 0.5$ AU, to show the detailed time evolution of accretion outbursts in general and to observe the inside-out bursts in particular.

Subject headings: accretion disks, stars: formation, stars: pre-main sequence

1. Introduction

The (re)discovery of the magnetorotational instability (MRI: e.g., Balbus & Hawley 1998, and references therein), appears to resolve the long-standing problem of the anomalous viscosity in sufficiently ionized accretion disks. To a crude approximation, this validates the use of Shakura & Sunyaev (1973) “ α viscosity” disks, though there are differences in detail (e.g., Balbus & Papaloizou 1999; Gammie 1996). Constant α disks have been employed in many situations, including the evolution of pre-main sequence disks (e.g., Hartmann et al. 1998). However, as pointed out by Gammie (1996), thermal ionization levels

¹Dept. of Astronomy, University of Michigan, 500 Church St., Ann Arbor, MI 48105

²Department of Astrophysical Sciences, Princeton University, 4 Ivy Lane, Peyton Hall, Princeton, NJ 08544

³Dept. of Astronomy, University of Illinois Urbana-Champaign, 1002 W. Green St., Urbana, IL 61801

⁴Dept. of Physics, University of Illinois Urbana-Champaign

in protostellar and protoplanetary disks generally are so low that it is unlikely that the MRI operates everywhere. Gammie suggested that transport in these regions might be limited to surface “active” layers, in which non-thermal ionization (cosmic rays, stellar X-rays) could allow the MRI to operate, while in the central regions of the disk there could be a non-viscous “dead zone”. A rich variety of phenomena are thus enabled beyond simple (quasi-steady) viscous disks (Vorobyov & Basu 2005, 2006, 2007, 2009; Zhu et al. 2010a,b; Martin & Lubow 2011; Martin et al. 2012a,b).

Gammie (1996) noted that if the MRI-active layer has a roughly constant surface density, the result is a pileup of material in the inner disk which eventually could become gravitationally unstable and result in a rapid burst of accretion, perhaps producing an FU Ori outburst (Hartmann & Kenyon 1996). While early models of FU Ori accretion events relied on traditional thermal instability theory (Clarke et al. 1990; Bell & Lin 1994), Zhu et al. (2007) showed that the rapidly-accreting region of FU Ori extends much further in radius from the central star than can be achieved with this theory. The very large amount of mass accreted in one of FU Ori’s outbursts ($\sim 10^{-2} M_{\odot}$) over such short timescales ($\sim 10^2$ yr) requires a large amount of material to be present in the disk at relatively small radii. This is a natural result of models in which gravitational instability (GI) triggers the outbursts (Armitage et al. 2001; Vorobyov & Basu 2006, 2007, 2009; Zhu et al. 2009c, 2010a,b; Martin & Lubow 2011; Martin et al. 2012a,b).

Zhu et al. (2010b) presented one-dimensional, two-layer evolutionary disk models including infall from a rotating protostellar cloud, and showed that they could qualitatively reproduce the main features of the outbursts of FU Ori and V1057 Cyg, with rapid rise times and slowly-decaying accretion. The simulations included irradiation from the central star, but did not take into account the accretion luminosity, which during outbursts can be far larger than the stellar photospheric radiation. While the geometry of disk accretion may not favor self-irradiation (Bell 1999), during infall the dusty opaque envelope will act as a blanket, reradiating a significant portion of the accretion luminosity toward the disk. In addition the Zhu et al. (2010b) calculations assumed that the central layer - the dead zone - had no viscosity unless it became gravitationally unstable. However, detailed shearing box simulations of the MRI in disks with a stratified structure and a resistivity that increases toward the midplane indicate that MHD turbulence generated in the upper MRI-active layers produces some hydrodynamic turbulence in the inactive layers (Fleming & Stone 2003; Okuzumi & Hirose 2011; Gressel et al. 2012). Furthermore, these investigations suggest that this turbulence creates Maxwell stresses, which result in a small but non-zero viscosity that can transport angular momentum outward and thus mass inward.

These considerations motivate further investigations of protostellar accretion using the two-layer one-dimensional model. We find that the position and properties of the inner boundary, the inclusion of irradiation by the accretion luminosity generated in the inner disk, and any non-zero dead zone viscosity have significant effects on the resulting bursts of mass accretion. Our treatment is sufficiently limited to preclude detailed predictions, but the qualitative behavior is suggestive, given that continuing observations of protostars and pre-main sequence stars are increasingly found to exhibit a wide variety of accretion events, beyond the large FU Ori outbursts (Hartmann & Kenyon 1996; Herbig 2008; Muzerolle et al. 2005; Reipurth & Aspin 2010; Aspin et al. 2010; Covey et al. 2011; Lorenzetti et al. 2012).

2. Methods

We use a modified version of the one-dimensional, two-zone disk model previously introduced in Zhu et al. (2010a,b), including changes to the infall model, enhanced disk heating, and viscosity in the dead zone. Here we review our scheme.

2.1. Surface density evolution

The surface density of a disk is evolved based on the mass and angular momentum conservation equations in cylindrical coordinates,

$$2\pi R \frac{\partial \Sigma_i}{\partial t} - \frac{\partial \dot{M}_i}{\partial R} = 2\pi g_i(R, t) \quad (1)$$

and

$$2\pi R \frac{\partial}{\partial t}(\Sigma_i R^2 \Omega) - \frac{\partial}{\partial R}(\dot{M}_i R^2 \Omega) = 2\pi \frac{\partial}{\partial R}(R^2 W_{R\phi, i}) + 2\pi \Lambda_i(R, t), \quad (2)$$

where Σ_i is the surface density, Ω is the angular frequency, \dot{M}_i is the radial mass flux, $W_{R\phi, i} = R \Sigma_i \nu_i d\Omega/dR$, and ν_i is the viscosity. The subscript i denotes either the active layer (“a”) or dead zone (“d”). The terms $2\pi g_i(R, t)$ and $2\pi \Lambda_i(R, t)$ are the mass and angular momentum flux per unit distance of infall material from an envelope cloud (Cassen & Moosman 1981). Then, assuming instantaneous centrifugal balance (see Zhu et al. 2010b), equations (1) and (2) can be simplified to

$$\dot{M}_i = 6\pi R^{1/2} \frac{\partial}{\partial R}(R^{1/2} \Sigma_i \nu_i) + \frac{2\pi R^2 \Sigma_i}{M_R} \frac{\partial M_R}{\partial t} - 4\pi \left(\frac{R}{GM_R} \right)^{1/2} (\Lambda_i(R, t) - g_i(R, t) R^2 \Omega(R)), \quad (3)$$

where M_R is the sum of the mass of the central star and the disk mass within R . We then sequentially solve Equations (3) and (1) to evolve the disk.

In Zhu et al. (2010b) mass and angular momentum were added to the disk using the infall model of Cassen & Moosman (1981),

$$g(R, t) = \frac{\dot{M}_{\text{in}}}{4\pi R_c} \left(1 - \frac{R}{R_c} \right)^{-1/2} \text{ if } R \leq R_c, \quad (4)$$

$$g(R, t) = 0 \text{ if } R > R_c, \quad (5)$$

and

$$\Lambda(R, t) = g(R, t) R \left(\frac{GM_c}{R_c} \right)^{1/2} \text{ if } R \leq R_c, \quad (6)$$

$$\Lambda(R, t) = 0 \text{ if } R > R_c. \quad (7)$$

Here R_c is the centrifugal radius, that is the outer radius at which mass is added to the disk at time t , and $\dot{M}_{\text{in}} = 0.975 c_s^3 / G$ is a constant total infall mass rate at a given cloud temperature (Shu 1977; Terebey et al. 1984). However, this model has a singularity at $R = R_c$; with finite grids this potentially causes non-convergent behavior at different grid resolutions. To avoid this we modified the infall model to eliminate the singularity by using a constant mass flux per unit distance.

Another problem occurs at the inner boundary, which is difficult to make very small because for numerical reasons (short time steps, dust evaporation, etc.) as well as fundamental uncertainties; for example, is the disk truncated by a stellar magnetosphere, and if so where, and is there an outflow from the inner disk edge. In addition, mass infall right at the inner boundary produces different results depending upon on precisely which inner boundary radius we choose. To minimize these problems we take inner boundary radii which are relatively small but still comfortably outside the expected point of magnetospheric truncation. We further assume that envelope material does not fall onto the disk inside $0.2R_c$, justified on the basis that the well-known emergence of jets and outflows seen in even the earliest protostellar phases should prevent the lowest-angular momentum material from reaching the disk or star (Reipurth & Bally 2001). By tying the inner radius of infall to R_c we effectively assume that the same streamline denotes the boundary between outflow and inflow, such that the outflow cone retains the same opening angle, in this case, a half-angle of 26.6° . This particular choice of opening angle is arbitrary and adopted mainly for numerical convenience.

The mass infall rate of the modified model is

$$g(R, t) = \frac{\dot{M}_{\text{in}}}{2\pi R_c} \text{ if } 0.2R_c \leq R \leq R_c \quad (8)$$

and

$$g(R, t) = 0 \text{ if } R < 0.2R_c \text{ or } R > R_c. \quad (9)$$

The corresponding angular momentum added to the disk per unit distance is

$$\Lambda(R, t) = g(R, t)R \left(\frac{GM_c}{R_c} \right)^{1/2} \text{ if } 0.2R_c \leq R \leq R_c \quad (10)$$

and

$$\Lambda(R, t) = 0 \text{ if } R < 0.2R_c \text{ or } R > R_c. \quad (11)$$

A comparison of the radial mass infall profile of our model to that of the Cassen & Moosman (1981) model is presented in Figure 5. In total, our model adds 11 % less angular momentum to the disk per unit mass infall than the Cassen & Moosman (1981) model. These modifications result in better convergence with increasing grid resolution.

2.2. Temperature evolution

The disk layer temperatures are determined by the balance between heating and radiative cooling. For the active layer, the energy equation is

$$\begin{aligned} C_{\Sigma, a} \partial_t T_a &= Q_{\text{heat}, a} - Q_{\text{cool}, a} \\ &= Q_{\text{vis}, a} + Q_{\text{infall}, a} + Q_{\text{grav}, a} + \frac{16}{3} \sigma \left(T_{\text{ext}}^4 \frac{\tau_a}{1 + \tau_a^2} + T_d^4 \frac{\tau_d}{1 + \tau_d^2} \right) \\ &\quad - \frac{16}{3} \sigma T_a^4 \left(\frac{\tau_a}{1 + \tau_a^2} + \frac{\tau_d}{1 + \tau_d^2} \right), \end{aligned} \quad (12)$$

where $C_{\Sigma,a} = \Sigma_a c_{s,a}^2 / T_a$ is the heat capacity of the active layer. Here T_{ext} characterizes the heating flux due to the irradiation of the disk by the stellar and (inner disk) accretion luminosity, and τ_a and τ_d are the optical depths of the active layer and the dead zone, respectively,

$$\tau_a = \frac{1}{2} \Sigma_a \kappa(\rho_a, T_a) \quad (13)$$

and

$$\tau_d = \frac{1}{2} \Sigma_d \kappa(\rho_d, T_d) \quad (14)$$

using the Rosseland mean opacity κ taken from Zhu et al. (2009a). In Equation (12), the first three terms are local heating of the active layer due to the viscosity, the infall, and the gravitational potential energy change, respectively. The fourth term consists of the external heating (see below) and the radiative heating from the underlying dead zone. The last term includes the radiative cooling toward each side of the active layer.

The energy equation of the dead zone is similar to that of the active layer,

$$C_{\Sigma,d} \partial_t T_d = Q_{\text{heat},d} - Q_{\text{cool},d}, \quad (15)$$

where $C_{\Sigma,d} = \Sigma_d c_{s,d}^2 / T_d$ is the heat capacity of the dead zone. If the active layer is optically thick, the energy equation is

$$C_{\Sigma,d} \partial_t T_d = Q_{\text{vis},d} + Q_{\text{infall},d} + Q_{\text{grav},d} + \frac{16}{3} \sigma T_a^4 \frac{\tau_d}{1 + \tau_d^2} - \frac{16}{3} \sigma T_d^4 \frac{\tau_d}{1 + \tau_d^2}. \quad (16)$$

On the other hand, if the active layer is optically thin, the incident flux from the outside of the dead zone would be $\sigma(\tau_a T_a^4 + T_{\text{ext}}^4)$ so that the energy equation is

$$C_{\Sigma,d} \partial_t T_d = Q_{\text{vis},d} + Q_{\text{infall},d} + Q_{\text{grav},d} + \frac{16}{3} \sigma(\tau_a T_a^4 + T_{\text{ext}}^4) \frac{\tau_d}{1 + \tau_d^2} - \frac{16}{3} \sigma T_d^4 \frac{\tau_d}{1 + \tau_d^2}. \quad (17)$$

Again, the first three terms in equations (16) and (17) represent local heating, while the last two terms account for radiative heating from the outside of the dead zone and the radiative cooling.

In the energy equations, the viscous heating is

$$Q_{\text{vis},i} = \frac{3}{2} W_{R\phi,i} \Omega, \quad (18)$$

where $W_{R\phi,i} = (3/2) \Sigma_i \nu_i \Omega$ and $\nu_i = \alpha_i c_{s,i}^2 / \Omega$. The viscosity parameter α_i is explained in detail in the next section.

During infall the added material has smaller specific angular momentum than the disk material at the same radius. This results in a readjustment of the disk such a way that material moves inward. As we are assuming effectively instantaneous centrifugal balance, the increase in the gravitational potential energy driven by the readjustment process must be accompanied by the corresponding energy release. Here we assume that this heats the active layer only ($Q_{\text{infall},d} = 0$), as this is the material directly impacted by the infalling matter. The heating by infalling material is then

$$Q_{\text{infall},a} = \frac{GM_* \dot{M}_{\text{in}}}{4\pi R_c^3} \frac{3 - 2\sqrt{(R/R_c)}}{(R/R_c)^2} \text{ if } 0.2R_c \leq R \leq R_c \quad (19)$$

and

$$Q_{\text{infall},a} = 0 \text{ if } R < 0.2R_c \text{ or } R > R_c. \quad (20)$$

As accretion proceeds, the central stellar mass increases and the disk gravitational potential energy will become more negative. In response, even in the absence of viscosity disk material will move inward, implying additional accretion luminosity. The heating by this effect is

$$Q_{\text{grav},i} = \frac{GM_* \dot{\Sigma}_i}{2R}, \quad (21)$$

where \dot{M}_* is change in the mass of the central star.

The irradiation flux can be written as

$$\sigma T_{\text{ext}}^4 = \frac{f_* L_*}{4\pi R^2} + \frac{f_{\text{acc}} L_{\text{acc}}}{4\pi R^2} + \sigma T_{\text{env}}^4, \quad (22)$$

where L_* and L_{acc} are the stellar luminosity and the accretion luminosity, respectively, and T_{env} is the envelope cloud temperature. The coefficients f_* and f_{acc} account for the non-normal irradiation of the disk surface. For the stellar irradiation we use $f_* = 0.1$ as in Zhu et al. (2010a) and assume the stellar luminosity follows the mass-luminosity relation

$$\log \left(\frac{L_*}{L_\odot} \right) = 0.20 + 1.74 \log \left(\frac{M_*}{M_\odot} \right) \quad (23)$$

which is an approximate power-law fit to pre-main sequence stars in the Taurus molecular cloud, using the luminosities and effective temperatures from Kenyon & Hartmann (1995), and adopting the Siess et al. (2000) evolutionary tracks to obtain the masses. The mass-luminosity relation is slightly modified from Zhu et al. (2010b).

The inclusion of external heating by inner disk accretion is another new feature of our calculations. The accretion luminosity is calculated as

$$L_{\text{acc}} = \frac{GM_* \dot{M}}{2R_\odot}, \quad (24)$$

where we assume a typical T Tauri stellar radius. In this case the appropriate value of f_{acc} is quite uncertain. At low to moderate accretion rates, magnetospheric accretion onto the star can occur at high latitudes, so that adoption of $f_{\text{acc}} = 0.1$, similar to that used for the stellar photospheric irradiation, seems reasonable. On the other hand, at high accretion rates, the spectra of FU Ori objects provide no indication of magnetospheric accretion (Hartmann & Kenyon 1996), and irradiation of the outer disk by a relatively flat inner disk should be much less effective (Bell 1999). However, if a substantial infalling envelope surrounds the disk, it can capture much of the accretion luminosity and reradiate a significant part toward the disk (Natta 1993). We therefore use both $f_{\text{acc}} = 0.1$ and 0.01 to examine the importance of this heating.

The last term in Equation (22) is the flux from the envelope cloud whose temperature is assumed to 20 K. Thus, the stellar luminosity irradiation Q_* and the accretion luminosity irradiation Q_{acc} on the active layer become

$$Q_* = \frac{16}{3} \frac{f_* L_*}{4\pi R^2} \frac{\tau_a}{1 + \tau_a^2} \quad (25)$$

and

$$Q_{\text{acc}} = \frac{16}{3} \frac{f_{\text{acc}} L_{\text{acc}}}{4\pi R^2} \frac{\tau_a}{1 + \tau_a^2}. \quad (26)$$

We note that the accretion luminosity irradiation Q_{acc} should be distinguished from the local viscous accretion heating Q_{vis} . The relative importance of the individual heating terms, and their effects, during disk evolution will be discussed in §3.

2.3. Disk Viscosity

The viscosity parameter α_i is the sum of the MRI viscosity parameter $\alpha_{M,i}$ and the GI viscosity parameter $\alpha_{Q,i}$. The MRI viscosity parameter is assumed to have a fixed value of α_{MRI} only if a region can sustain the MRI. Thus, the active layer viscosity parameter is always set to $\alpha_{M,a} = \alpha_{MRI}$ while the dead zone has MRI viscosity only if the midplane temperature is higher than a critical temperature T_{MRI} to produce sufficient ionization levels. For the dead zone, we consider a residual viscosity as well as MRI viscosity and GI viscosity, $\alpha_d = \alpha_{M,d} + \alpha_{Q,d} + \alpha_{\text{rd}}$.

The idea of the dead zone residual viscosity (DZRV) α_{rd} is based on recent numerical magnetohydrodynamic simulations suggesting that magnetic turbulence in the active layers can drive hydrodynamic turbulence in the dead zone, implying a non-zero residual viscosity parameter $\sim 10^{-3} - 10^{-5}$ (Bai & Stone 2011; Okuzumi & Hirose 2011; Gressel et al. 2012). Thus, for non-zero DZRV model we set

$$\alpha_{\text{rd}} = \min \left(10^{-4}, f_{\text{rd}} \alpha_{MRI} \frac{\Sigma_a}{\Sigma_d} \right), \quad (27)$$

where f_{rd} is the efficiency of accretion in the dead zone whose value is chosen to be ≤ 1 ; this is intended to limit the effect of the active-layer induced turbulence such that the mass accretion rate of the dead zone (approximately) does not exceed that of the active layer ($\dot{M}_d \leq \dot{M}_a$). This seems intuitively reasonable. We consider the upper limit $f_{\text{rd}} = 1$ and consider a case with $f_{\text{rd}} = 0.1$ as it is unlikely that the active layer can be that effective in driving accretion.

Finally, the GI viscosity parameter is the same as in Zhu et al. (2010a),

$$\alpha_{Q,i} = e^{-Q^2}, \quad (28)$$

where Q is the Toomre parameter.

3. Results

3.1. Initial conditions

We start with a $0.1 M_{\odot}$ central protostar surrounded by an $M_c = 1 M_{\odot}$ cloud. We parameterize the cloud rotation in terms of $\omega = \Omega_c / \Omega_b$, where Ω_c is the (constant) angular frequency of the initial cloud, and

$\Omega_b = 2^{3/2} c_s^3 / GM_c$ is the breakup angular frequency at the outer cloud edge, and c_s is the (uniform) cloud sound speed. Our fiducial models assume $\omega = 0.03$, which results in $\sim 15\%$ larger cloud angular frequency than that used in the fiducial model of Zhu et al. (2010b) ($\Omega_c \sim 1.15 \times 10^{-14}$ rad s $^{-1}$ in our model). We set the maximum non-thermally ionized surface density Σ_A to 100 g cm $^{-2}$ for our fiducial choice and assume it is constant. We assume $T_{\text{MRI}} = 1500$ K and $\alpha_{\text{MRI}} = 0.01$ for all calculations. We adopt a cloud envelope temperature of $T_{\text{env}} = 20$ K, which yields a constant infall rate of $\sim 3.4 \times 10^{-6} M_\odot \text{yr}^{-1}$. This is 20 % smaller than the infall rate for conventional singular isothermal collapse model (Shu 1977) because of our modified infall model (see §2.1). The infall lasts for ~ 0.24 Myr, adding $0.8 M_\odot$ to the central star + disk in total.

3.2. Zero dead zone viscosity model

Zhu et al. (2010a) found that GI moves matter from the outer disk to the inner disk, leading to a pileup at $R \sim 2$ AU because GI is increasingly ineffective at small radii. Eventually enough material piles up to trap thermal energy that makes $T_d > T_{\text{MRI}}$, turns on the MRI thermally in the dead zone, and thus produces an outburst of accretion. Zhu et al. (2010b) investigated the long-term evolution of such disks and found that the evolution can be divided into three stages. The evolution starts with a quasi-steady disk accretion since the infall is to small radii where the inner disk can become hot enough to sustain the MRI thermally. Then, it turns into the outburst stage as the infall occurs at radii > 1 AU. After infall stops, the disk enters the T Tauri phase, having only a few GI-driven outside-in outbursts with a low mass accretion rate in between bursts.

Figure 2 shows the mass accretion rate and the mass of the central star, the disk, and the central star + disk as a function of time. The modified infall model and additional heating sources discussed in §2 produce no qualitative difference in the overall evolution from Zhu et al. (2010b).

The new heating sources for the first 0.3 Myr of the evolution at $R = 1$ and 10 AU are presented in Figures 3 and 4, together with the previously considered sources. In these figures, newly added terms in this paper are plotted in color while other terms have considered in Zhu et al. (2010a) and drawn in black. As one can see, heating by the change in gravitational energy is usually several orders of magnitude smaller than other terms so that it makes no change in the evolution. Infall heating provides comparable amount of heat to the active layer but is only limited to the region material falls onto, increasing the local disk temperature slightly. However, the large increase in the accretion luminosity during outburst produces enough irradiation to make the outer disk temperature increase dramatically. This is shown in Figure 5, where we show the mass accretion rate during a single outburst and the radial profiles of the disk surface density and the midplane temperature before outburst, at the maximum accretion rate, and at the end of the outburst. The temperature increase at the outer disk during outbursts does not affect the long-term evolution, because the viscous time of the outer regions ($\sim 10^5$ yr) is much longer than the outburst timescale of $\sim 10^3$ yr.

We also call attention to the jump in temperature at radii < 0.5 AU, which is due to thermal instability (Zhu et al. 2010a). This increase in temperature, which affects the behavior of the outburst of accreting material onto the central star, would not have been found if we had taken an inner radius of $\gtrsim 1$ AU (see discussion in §4).

The GI-driven outside-in bursts accrete $\sim 0.027 M_{\odot}$ of material onto the central star and last for ~ 1340 years on average. Although the duration obtained in our calculation is longer than the typical outburst timescale seen in FU Ori, the timescale of an outburst can be scaled with a choice of α_{MRI} since $\Delta t_{\text{burst}} \sim R^2/\nu \propto \alpha_{\text{MRI}}^{-1}$ (see Zhu et al. 2010a). The outside-in bursts are rare, because the disk needs a lot of material to trigger MRI through GI while it is difficult to do so with zero DZRV. The duty cycle of this model is thus pretty small, ~ 0.06 during outburst stage and ~ 0.005 during T Tauri phase. The details of disk properties at 0.24 and 1 Myr and of outside-in bursts are summarized in Table 1. All the outburst quantities in the table are time-averaged values after the initial quasi-accretion phase while those vary with time.

3.3. Non-zero dead zone residual viscosity model

While the modified infall model and additional heating sources with zero DZRV make no qualitative change in the overall evolution, a finite DZRV makes a lot of difference in the long-term evolution and in the single outburst behavior as well. Figure 6 shows the mass accretion rate and the mass of the central star, the disk, and the central star + disk as a function of time. During infall the disk has a quasi-steady accretion phase at the beginning ($t \lesssim 0.08$ Myr) and the outburst stage follows, as in the zero DZRV case. However, the evolution after the accretion phase is different in that the non-zero DZRV model shows a lot of smaller outbursts instead of a few large outbursts.

Figure 7 and 8 show the heating sources of active layer and dead zone of the non-zero DZRV model at $R = 1$ and 10 AU, respectively. The major difference between this model and the zero DZRV model is that dead zone viscous heating provides a significant amount of heat at the inner disk even after infall ends. We have run calculations with different T_{MRI} (1300 K and 1800 K) and found that the overall features are not sensitive to the choice of T_{MRI} . At the outer disk, the accretion luminosity irradiation is still important during bursts while the temperature increase is not as dramatic as in the zero DZRV model due to lower accretion peak. Infall and gravitational heating are less important than others.

Figure 9(a) shows the mass accretion rate during a single outburst with non-zero DZRV. Radial surface density and midplane temperature profiles at the beginning, at the maximum accretion rate, and at the end of the burst are presented in Figure 9(b) and (c). The accretion behavior during a single outburst is remarkably different from that of the zero DZRV model. The outburst has a peak of $\dot{M}_{\text{max}} \sim 10^{-5} M_{\odot} \text{yr}^{-1}$, which is about two orders of magnitude smaller than that of the outside-in bursts. In addition, the accretion rate initially shows a rapid increase but has a slow rise time to its peak and a slow decrease after the peak as well. In this model, the dead zone is able to transport material with the help of the non-zero DZRV. Thus, the inner disk can be heated viscously and outbursts are initiated at the inner boundary of the disk before the GI piles up enough material at the middle of the disk ($R \sim 2$ AU) to initiate the MRI, which is the case for outside-in bursts. The ionization front propagates out to several AU from the inner boundary. Since the inside-out bursts have an MRI active inner boundary from their initiation, the disk continues to dump material from its innermost part during the whole bursts. Therefore, the system is not able to show a huge accretion rate as seen in outside-in bursts, but only generates moderate accretion rate. Note again that the

outburst triggers first at small radii, inside of ~ 0.5 AU (§4).

On average, the mass accreted onto the central star during a single inside-out burst is $\sim 1.5 \times 10^{-3} M_{\odot}$ and it lasts ~ 450 years. The inside-out bursts occur frequently enough to get a duty cycle of ~ 0.16 during outburst stage and ~ 0.06 during T Tauri phase. The disk properties and outburst details of the non-zero DZRV model are summarized in Table 1.

3.4. Efficiency of accretion luminosity irradiation

As shown in the previous sections, irradiation by the inner disk plays an important role during outburst on the temperature profile at the outer disk. However, the efficiency of the accretion luminosity irradiation is uncertain as far as the non-normal irradiation of the disk is considered. We thus test the effect of changing f_{acc} to 0.01, which is ten times smaller than the fiducial value.

We found essentially no change in the overall evolution of both zero and non-zero DZRV cases, since the accretion luminosity irradiation is several orders of magnitude smaller than main heating sources - active layer viscous heating and stellar irradiation - during the quiescent phase. During outbursts, however, the accretion luminosity irradiation still dominates the heating even with a ten times smaller efficiency, making a significant difference to the outer disk temperature. Not surprisingly, the increase in outer disk temperature during bursts is smaller than the standard cases by a factor of ~ 2 .

3.5. Accretion Efficiency in Dead Zone

Intuitively, it seems unlikely that the turbulence generated by the active layers within the dead zone can transport as much mass as the active layer (e.g., Hartmann et al. 2006). In our models this happens when $\alpha_{\text{rd}} \gtrsim 10^{-4}$, where $\Sigma_d \gtrsim 10^5 \text{ g cm}^{-2}$. This could be an overestimate of the efficiency with which the MRI turbulence in the active layers drives accretion in the dead zone. We therefore adjust the dead zone accretion efficiency f_{rd} to 0.1 so that dead zone only has an accretion rate of ~ 10 % of the active layer at most.

Figure 10 shows the mass accretion rate and the mass of the central star, the disk, and the central star + disk as a function of time. Initially, the evolution resembles that of the standard zero DZRV model rather than the non-zero DZRV model; the system shows a distinct outburst phase during infall. This is because the mass that the dead zone can carry is now limited and thus generates less viscous heating at small radii than the standard non-zero DZRV case. Therefore, mass piles up at large radii through the GI before inner disk gets heated and triggers inside-out bursts. After infall ends, however, we still see inside-out bursts with much less frequency than the standard non-zero DZRV model, which is again due to less viscous heating at the inner disk. The duty cycle during T Tauri phase of this model is only 0.015, which is four times smaller than that of the standard non-zero DZRV model. First three outbursts after infall ends are outside-in bursts, since disk already collects enough material at outer disk during infall to make them. This emphasizes importance of understanding the effect of MRI turbulence on dead zones (§4).

3.6. Dependence on Σ_A and α_{MRI}

While we use $\Sigma_A = 100 \text{ g cm}^{-2}$ as our fiducial value, several studies have pointed out that the active layer more likely has a lower surface density (e.g. Sano et al. 2000; Bai & Goodman 2009). We thus test $\Sigma_A = 20 \text{ g cm}^{-2}$ and adjust the MRI viscosity parameter $\alpha_{MRI} = 0.05$ to maintain roughly the same mass accretion rate ($\dot{M} \propto \alpha \Sigma$) during the quiescent phase as the standard cases (and also in agreement with typical T Tauri accretion rates).

Figure 11 shows the mass accretion rates of both zero and non-zero DZRV models adopting the lower value of Σ_A . The mass accretion rate during a single outburst and radial surface density and midplane temperature profiles at the beginning, at the maximum accretion rate, and at the end of a single outburst of the both models are presented in Figure 12. Since the outburst timescale depends on the MRI viscosity parameter ($\Delta t_{\text{burst}} \propto \alpha_{MRI}^{-1}$), the details of the outbursts, such as outburst duration and peak accretion rate, vary. However, the overall evolution as well as the initiation of outbursts remain the same. We see GI-induced MRI-driven outside-in bursts in the zero DZRV case and viscously triggered inside-out bursts in the non-zero DZRV case. This is because the overall evolution and the initiation of outbursts are governed by the mass accretion during the quiescent phase, which we manage to be unchanged. We note that the shorter timescales are in better agreement with FU Ori (see Zhu et al. 2007). The disk properties and outburst details are summarized in Table 1.

4. Discussion

Our simulations show that it is possible to obtain inside-out triggering of accretion outbursts as well as outside-in bursts (e.g., Zhu et al. 2010a,b), with the former enhanced if there is finite dead zone residual viscosity. The two types of outbursts were also obtained in the model developed by Bell & Lin (1994; BL) for FU Ori outbursts. In the BL model, the outbursts were due to thermal instability (TI), plus an assumed increase in α from a very low value to a much higher value. As Zhu et al. (2007, 2008) showed, the TI model is inconsistent with observations of FU Ori, because the high temperatures required limit the region of rapid accretion to smaller radii than inferred from modeling the spectral energy distribution including Spitzer Space Telescope data. Nevertheless, the finite dead zone residual viscosity models are qualitatively similar to the basic feature of the BL models which produce inside-out bursts; a small but finite viscosity allows material in the inner disk to produce enough trapping of viscously-generated heat to trigger a higher viscosity and eventually an outburst. As BL showed, such inner disk triggering leads to outbursts with slow rise times, qualitatively consistent with the observed outburst of V1515 Cyg (Herbig 1977; M. Ibrahimov, personal communication).

BL showed that outbursts with rapid rise times, such as observed in FU Ori and V1057 Cyg (Herbig 1977), required outside-in accretion events. In the BL model, a large outer perturbation of the disk was required. In modern models, the event is triggered by GI, which piles up material at larger radii than possible in the TI model (Armitage et al. 2001; Vorobyov & Basu 2006, 2007, 2009, 2010; Zhu et al. 2010a,b; Martin et al. 2012a,b). Our current results build upon those of Zhu et al. (2010b) in that we clearly identify

some inside-out bursts during the main phase of infall (they were actually present in the Zhu et al. simulation as well but were not emphasized).

Our results also bear similarities to outbursts in models of cataclysmic variables (CV). Two different types of outbursts (outside-in and inside-out) in accretion disks around dwarf novae were first predicted by Smak (1984). In CV models, mass transfer from the secondary rises the effective temperature of a disk annulus to 5000–8000 K, which corresponds to hydrogen recombination inside the disk and thus triggers the TI (Menou et al. 1999). While the dead zone residual viscosity parameter is the feature that changes outburst behavior in our model, CV models use the mass transfer rate to generate two different outbursts. If the mass transfer rate is high, the accumulation timescale of transferred material is shorter than the viscous timescale, allowing material piles up at outer disk. Thus, outside-in bursts are triggered. In contrast, if mass transfer rate is low, the accumulation timescale becomes longer than the viscous timescale so that the outbursts outside-in outbursts are replaced by inside-out ones. The resulting outburst behaviors of CV models are similar to ours; inside-out bursts have a smaller accretion peak and a slower rise time than outside-in ones (see Figures 3 and 4 of Hameury et al. 1998).

It is worth emphasizing that the outburst behavior of systems, observed at optical and near-infrared wavelengths, is a result of accretion onto or near the star, i.e. at radial scales $\lesssim 0.1$ AU. While our models do not reach magnetospheric or stellar radii, our inner boundary radius of 0.2 AU is small enough to capture behavior (thermal instability, inside-out bursts) which cannot be seen in simulations with inner boundaries > 1 AU. Thus, while our own treatment of non-steady accretion has its limitations, time histories of accretion in simulations with large inner disk radii must be treated with special caution. Using an inner boundary of a few AU, as in the series of papers by Vorobyov & Basu (2006, 2007, 2009) or Dunham & Vorobyov (2012), one would not find the outburst behavior characterized by our models or those of Armitage et al. (2001) or Martin et al. (2012a,b).

Along these lines, we have found that the precise duration of the inside-out bursts during infall is sensitive function of the value of the inner radius. We do not explore this further here because there are other major uncertainties in our treatment, such as the assumption of a constant active layer surface density, the characterization of the GI via an α viscosity, and the way in which we implement a finite dead zone viscosity. In the following paragraphs we discuss these issues in turn.

Advanced MHD treatments of the active layer are complex and involve a number of unknowns, such as whether low-energy cosmic rays can penetrate the accretion-driven winds, grain growth and settling, the presence of metal ions, etc. (e.g., Sano et al. 2000; Ilgner & Nelson 2006, 2008; Hirose & Turner 2011; Perez-Becker & Chiang 2011). Martin et al. (2012a,b) argue that a large critical Reynolds number is necessary for transport to occur, resulting “active” regions very different than the constant Σ_a we use. However, Martin et al. (2012b) predict essentially no accretion onto the central star in between outbursts, whereas the pre-outburst spectrum of V1057 Cyg shows emission lines typical of T Tauri stars accreting at $\sim 10^{-8} M_{\odot} \text{ yr}^{-1}$ (Herbig 1977). More recently, Miller et al. (2011) showed that the classical (accreting) T Tauri star LkHa 188-G4 underwent an FU Ori-type eruption in 2009. Finally, a pre-outburst spectrum of the FU Ori object V733 Cep (Reipurth et al. 2007) also showed characteristic accreting T Tauri emission lines

(B. Reipurth, personal communication). Thus the pre-outburst state of at least some FU Ori objects is one of accretion at rates typical of T Tauri stars, which we obtain with our adopted value of $\alpha_d \Sigma_d$, at least in the inner disk.

Similarly, our treatment of the GI with an α viscosity is crude; as in the case of the MRI, three-dimensional simulations are required to treat the GI properly (e.g., Rice et al. 2003; Boley et al. 2006; Durisen et al. 2007, and references therein). Two-dimensional simulations also do a better job of capturing the GI than our treatment (e.g., Vorobyov & Basu 2006, 2007, 2009, 2012). However, as pointed out by Zhu et al. (2009), and as shown in Zhu et al. (2010a,b) and the present simulations, the GI becomes harder and harder to sustain as one moves to smaller radii, whereas triggering of the MRI becomes easier.

Finally, the presence and behavior of non-zero viscosity in dead zones is highly uncertain. While simulations of resistive, stratified disks in shearing boxes appear to show that the active layer produces a non-zero α in the central “dead” layers (Fleming & Stone 2003; Okuzumi & Hirose 2011; Gressel, Nelson, & Turner 2012), the level to which this occurs, the amount of mass transport involved, and precisely where energy is dissipated is unclear. For example, our model assumes that the wave energy is dissipated near the midplane, and thus the heat generated can be trapped radiatively by the opacity of the disk at the midplane; however, it is possible that dissipation is concentrated at higher levels (N. Turner, personal communication).

In all, these uncertainties show that our current results must be taken as suggestive rather than predictive for variations of accretion in young stellar objects. Nevertheless, these simple models, which can be evolved easily for significant evolutionary timescales, illustrate the potential information on transport processes in protostellar and protoplanetary disks that might ultimately be gleaned from the observed accretion outbursts. Due to the increasing monitoring of young stellar objects, it is becoming increasingly clear that a wide variety of accretion behavior is exhibited in young stars, emphasizing that further progress on challenging problems of globally simulating MRI and GI in protostellar disks may pay rich dividends.

5. Summary

In this paper, we have extended the one-dimensional, two-zone model of long-term protostellar disk evolution with infall, which is previously introduced in Zhu et al. (2010a,b). Our modified models include a revised treatment of infall, enhanced disk heating, and possible non-zero viscosity in the dead zone. While the former two changes produce no qualitative difference in the overall evolution from the Zhu et al. (2010b), we find that the presence of a small but finite dead zone viscosity can trigger inside-out bursts initiated at or near the inner edge of the disk through dead zone viscous heating, instead of GI-induced MRI-driven outside-in bursts with zero dead zone viscosity. These inside-out bursts not only bear a qualitative resemblance to the outburst behavior of one FU Ori objects, V1515 Cyg, but emphasize a careful treatment of the inner disk regions in simulations.

Given the uncertainties, our results are rather suggestive than predictive. However, two types of outbursts seen in FU Ori objects can be successfully reproduced by the simple α treatment in the dead zone. This difference in accretion behavior could be a potential probe of transport efficiency in the dead zone.

We acknowledge useful conversations with Bo Reipurth and Neal Turner. This work was supported in part by NASA grant NNX08A139G and by the University of Michigan.

REFERENCES

- Alexander, R. D., & Armitage, P. J. 2007, MNRAS, 375, 500
- Armitage, P. J., Livio, M., & Pringle, J. E. 2001, MNRAS, 324, 705
- Aspin, C. 2011, AJ, 142, 135
- Aspin, C., Reipurth, B., Herczeg, G. J., & Capak, P. 2010, ApJ, 719, L50 (V1647)
- Bai, X.-N. & Goodman, J. 2009, ApJ, 701, 737
- Bai, X.-N. & Stone, J. M. 2011, ApJ, 736, 144
- Balbus, S. A., & Hawley, J. F. 1998, Reviews of Modern Physics, 70, 1
- Balbus, S. A., & Papaloizou, J. C. B. 1999, ApJ, 521, 650
- Bell, K. R. 1999, ApJ, 526, 411
- Bell, K. R., & Lin, D. N. C. 1994, ApJ, 427, 987
- Bell, K. R., Lin, D. N. C., Hartmann, L. W., & Kenyon, S. J. 1995, ApJ, 444, 376
- Boley, A. C., Mejía, A. C., Durisen, R. H., et al. 2006, ApJ, 651, 517
- Briceño, C., Vivas, A. K., Hernández, J., et al. 2004, ApJ, 606, L123
- Cassen, A. & Moosman, A. 1981, Icarus, 48, 353
- Clarke, C. J., Lin, D. N. C., & Pringle, J. E. 1990, MNRAS, 242, 439
- Covey, K. R., Hillenbrand, L. A., Miller, A. A., et al. 2011, AJ, 141, 40
- Dullemond, C. P., & Dominik, C. 2004, A&A, 421, 1075
- Dunham, M. M., & Vorobyov, E. I. 2012, ApJ, 747, 52
- Durisen, R. H., Boss, A. P., Mayer, L., et al. 2007, Protostars and Planets V, 607
- Fleming, T., & Stone, J. M. 2003, ApJ, 585, 908
- Gammie, C. F. 1996, ApJ, 457, 355
- Gressel, O., Nelson, R. P., & Turner, N. J. 2012, MNRAS, 422, 1140

- Hameury, J.-M., Menou, K., Dubus, G., Lasota, J.-P., & Huré, J.-M. 1998, MNRAS, 298, 1048
- Hartmatnn, L., Calvet, N., Gullbring, E., & D’Alessio, P. 1998, ApJ, 495, 385
- Hartmann, L., D’Alessio, P., Calvet, N., & Muzerolle, J. 2006, ApJ, 648, 484
- Hartmann, L. 2009, *Accretion Processes in Star Formation: Second Edition*, (Cambridge University Press)
- Hartmann, L., & Kenyon, S. J. 1996, ARA&A, 34, 207
- Herbig, G. H. 1977, ApJ, 217, 693
- Herbig, G. H. 2008, AJ, 135, 637
- Hirose, S., & Turner, N. J. 2011, ApJ, 732, L30
- Ilgner, M., & Nelson, R. P. 2006, A&A, 455, 731
- Ilgner, M., & Nelson, R. P. 2008, A&A, 483, 815
- Lorenzetti, D., Antoniucci, S., Giannini, T., et al. 2012, ApJ, 749, 188
- Martin, R. G., & Lubow, S. H. 2011, ApJ, 740, L6
- Martin, R. G., Lubow, S. H., Livio, M., & Pringle, J. E. 2012, MNRAS, 420, 3139
- Martin, R. G., Lubow, S. H., Livio, M., & Pringle, J. E. 2012, MNRAS, 423, 2718
- Menou, K., Hameury, J.-M., & Stehle, R. 1999, MNRAS, 305, 79
- Miller, A. A., Hillenbrand, L. A., Covey, K. R., et al. 2011, ApJ, 730, 80
- Muzerolle, J., Megeath, S. T., Flaherty, K. M., et al. 2005, ApJ, 620, L107
- Natta, A. 1993, ApJ, 412, 761
- Okuzumi, S., & Hirose, S. 2011, ApJ, 742, 65
- Perez-Becker, D., & Chiang, E. 2011, ApJ, 735, 8
- Reipurth, B., & Aspin, C. 2010, *Evolution of Cosmic Objects through their Physical Activity*, 19
- Reipurth, B., & Bally, J. 2001, ARA&A, 39, 403
- Rice, W. K. M., Armitage, P. J., Bate, M. R., & Bonnell, I. A. 2003, MNRAS, 339, 1025
- Sano, T., Miyama, S. M., Umebayashi, T., & Nakano, T. 2000, ApJ, 543, 486
- Shakura, N. I., & Sunyaev, R. A. 1973, A&A, 24, 337
- Shu, F. H. 1977, ApJ, 214, 488

- Smak, J. 1984, *Acta Astron.*, 34, 161
- Tanaka, H., Himeno, Y., & Ida, S. 2005, *ApJ*, 625, 414
- Terebey, S., Shu, F. H., & Cassen, P. 1984, *ApJ*, 286, 529
- Vorobyov, E. I., & Basu, S. 2005, *ApJ*, 633, L137
- Vorobyov, E. I., & Basu, S. 2006, *ApJ*, 650, 956
- Vorobyov, E. I., & Basu, S. 2007, *MNRAS*, 381, 1009
- Vorobyov, E. I., & Basu, S. 2009, *MNRAS*, 393, 822
- Vorobyov, E. I., & Basu, S. 2010, *ApJ*, 719, 1896
- Vorobyov, E. I. 2009, *ApJ*, 704, 715
- Zhu, Z., Hartmann, L., Calvet, N., Hernandez, J., Muzerolle, J., & Tannirkulam, A.-K. 2007, *ApJ*, 669, 483
- Zhu, Z., Hartmann, L., Calvet, N., Hernandez, J., Tannirkulam, A.-K., & D’Alessio, P. 2008, *ApJ*, 684, 1281
- Zhu, Z., Espaillat, C., Hinkle, K., Hernandez, J., Hartmann, L., & Calvet, N. 2009a, *ApJ*, 694, L64
- Zhu, Z., Hartmann, L., & Gammie, C. 2009b, *ApJ*, 694, 1045
- Zhu, Z., Hartmann, L., Gammie, C., & McKinney, J. C. 2009c, *ApJ*, 701, 620
- Zhu, Z., Hartmann, L., Gammie, C. F., Book, L. G., Simon, J. B., & Engelhard, E. 2010a, *ApJ*, 713, 1134
- Zhu, Z., Hartmann, L., & Gammie, C. F. 2010b, *ApJ*, 713, 1143

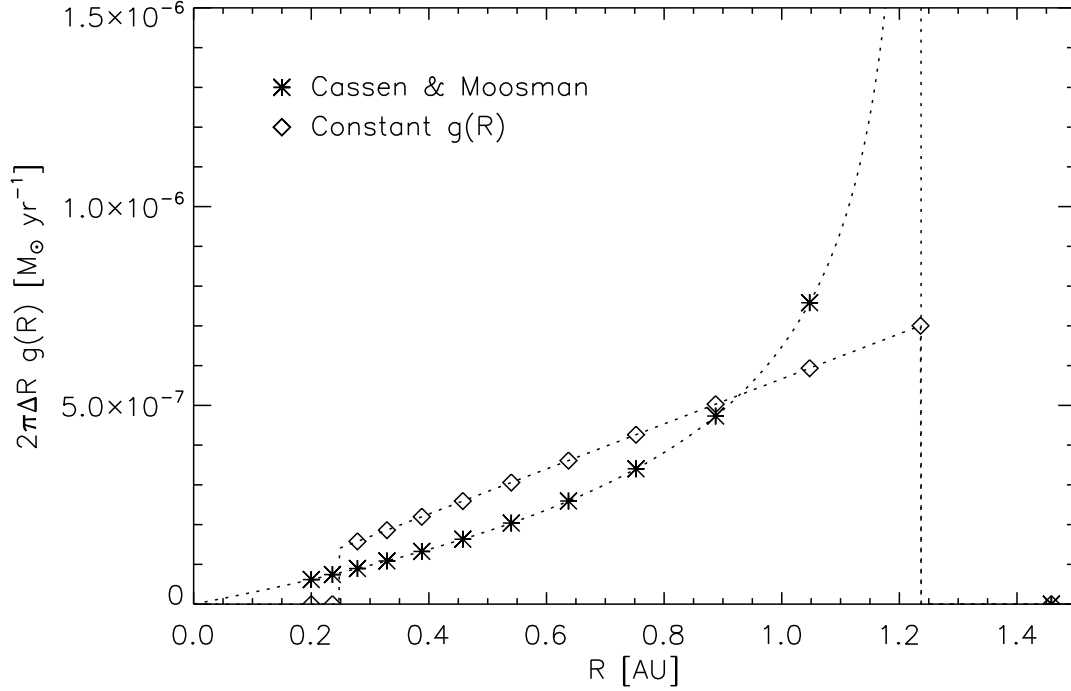


Fig. 1.— The mass infall rate at $t = 0.05$ Myr of Cassen & Moosman (1981) model (asterisks) and our constant $g(R)$ model (diamonds). The centrifugal radius at the time is $R_c \sim 1.24$ AU. Cassen & Moosman (1981) model gives $\sim 1.3 \times 10^{-5} M_\odot \text{ yr}^{-1}$ of mass infall rate at the nearest grid to R_c , which is about an order of magnitude large to be fitted in the figure. The mass infall rate inside $0.2 R_c$ is set to zero in our model to imitate protostellar outflows (see text). Dotted curves show analytic estimates of the mass infall rate of each model.

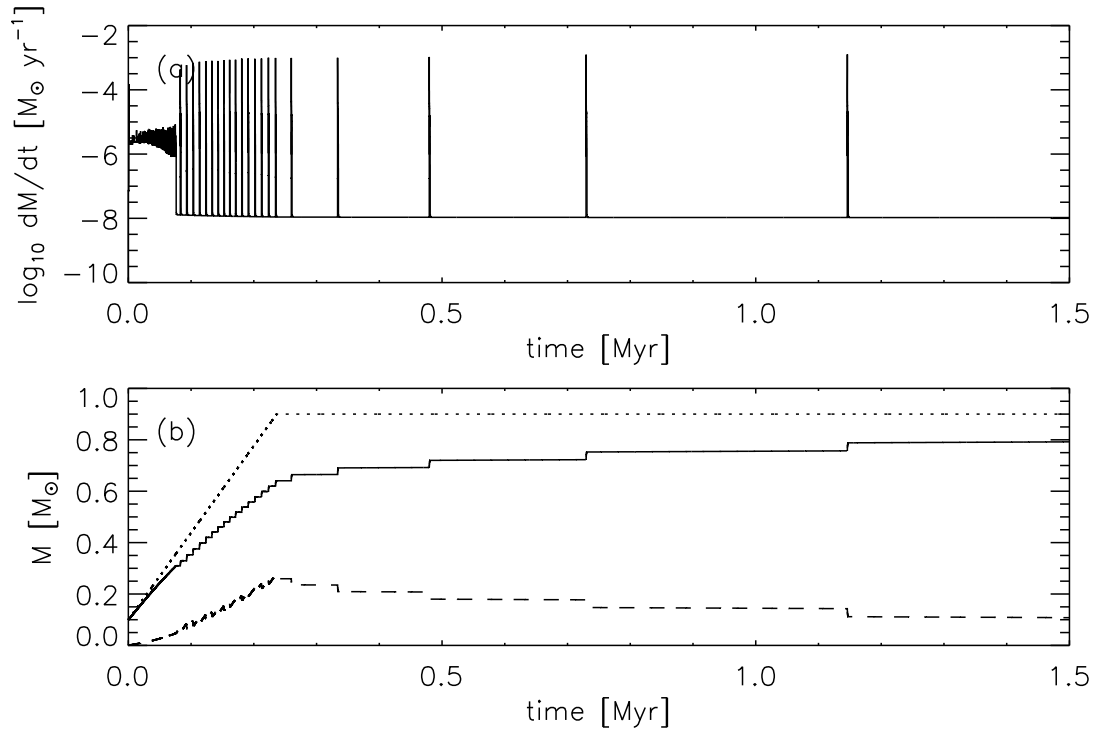


Fig. 2.— (a) Mass accretion rate and (b) mass of the central star + disk (dotted curve), mass of the central star (solid curve), and mass of the disk (dashed curve) with time for the standard zero DZRV model.

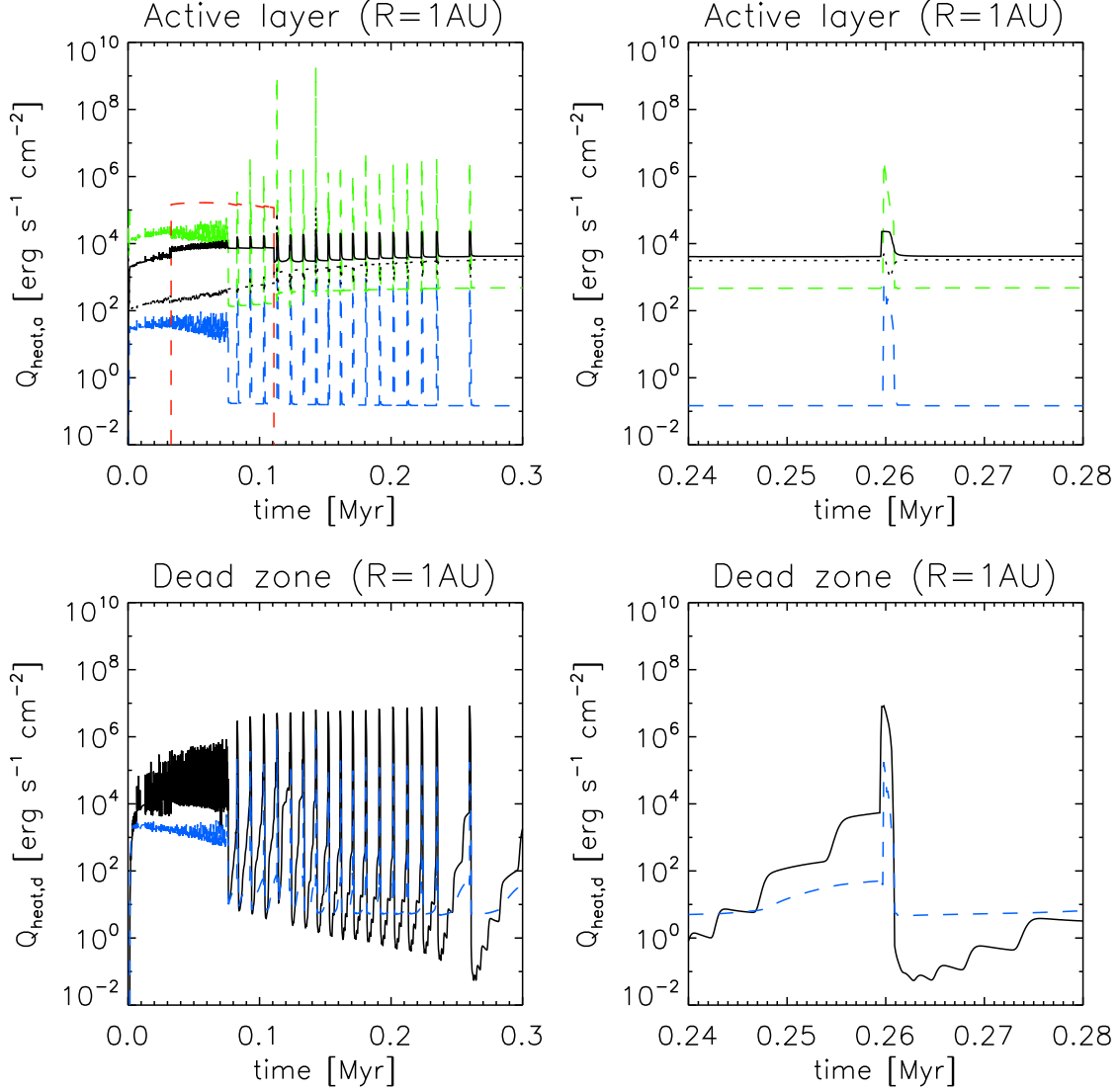


Fig. 3.— Various heating sources of the active layer (upper panels) and the dead zone (lower panels) at $R = 1$ AU for the first 0.3 Myr (left panels) and during a single outburst (right panels) with zero DZRV. Newly added heating sources in this paper are plotted in color while the heating sources have considered in (Zhu et al. 2010a,b) are presented with black curves. Upper panels: $Q_{\text{vis},a}$ (black solid), Q_* (black dotted), Q_{infall} (red dashed), Q_{acc} (green dashed), and $Q_{\text{grav},a}$ (blue dashed) are presented. Lower panels: $Q_{\text{vis},d}$ (black solid) and $Q_{\text{grav},d}$ (blue dashed) are presented.

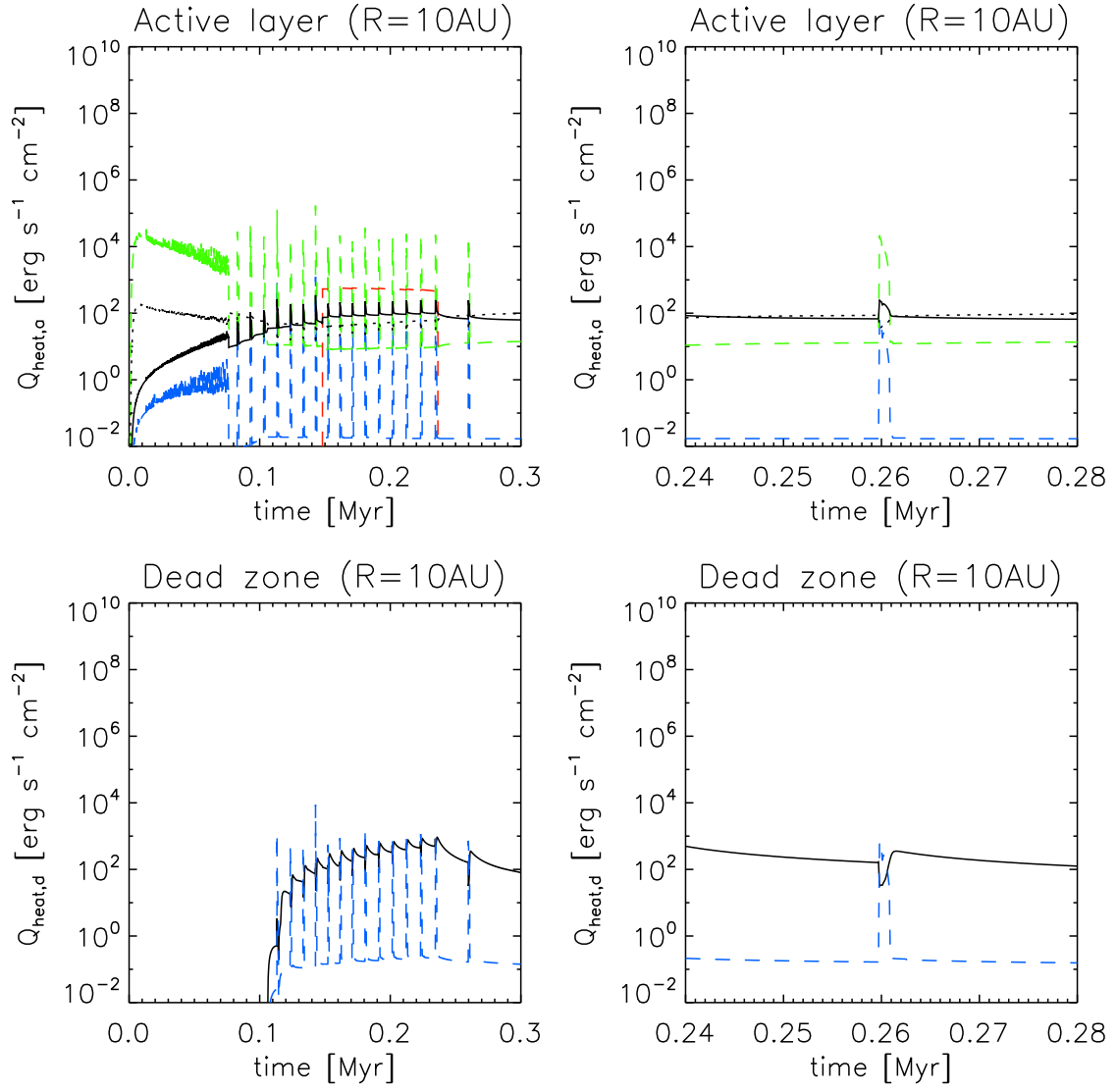


Fig. 4.— Same as Figure 3 but at $R = 10$ AU.

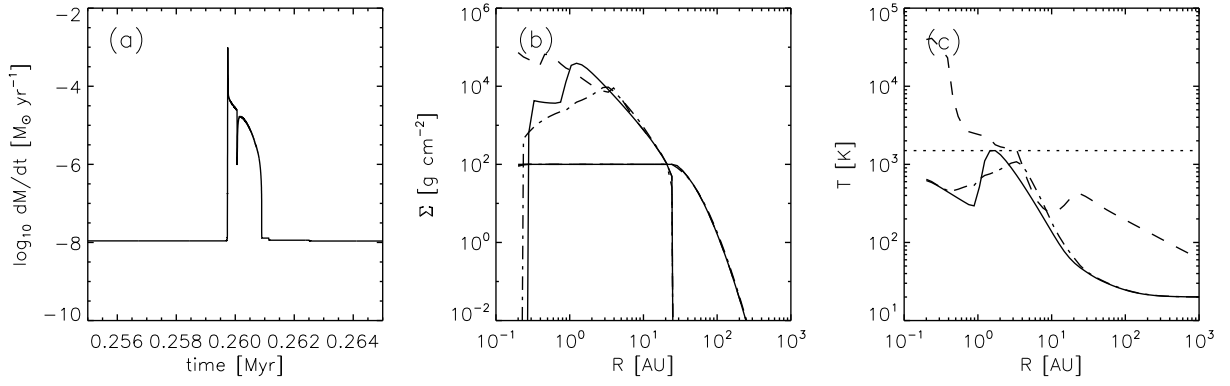


Fig. 5.— (a) Mass accretion rate of a single outburst of the standard zero DZRV model. The “drop out” in accretion during the middle of the outburst is an artifact of the one-dimensional treatment (Zhu et al. 2010a). Radial profiles of (b) the surface densities and (c) the midplane temperatures before the outburst (solid curves), at the maximum accretion rate (dashed curves), and at the end (dash-dotted curves) of the burst are plotted. In panel (b), the curves with higher surface densities at the inner disk represent the dead zone surface density while the lower ones extend further out represent the active layer. In panel (c), the dotted horizontal line represents the MRI activation temperature $T_{\text{MRI}} = 1500$ K.

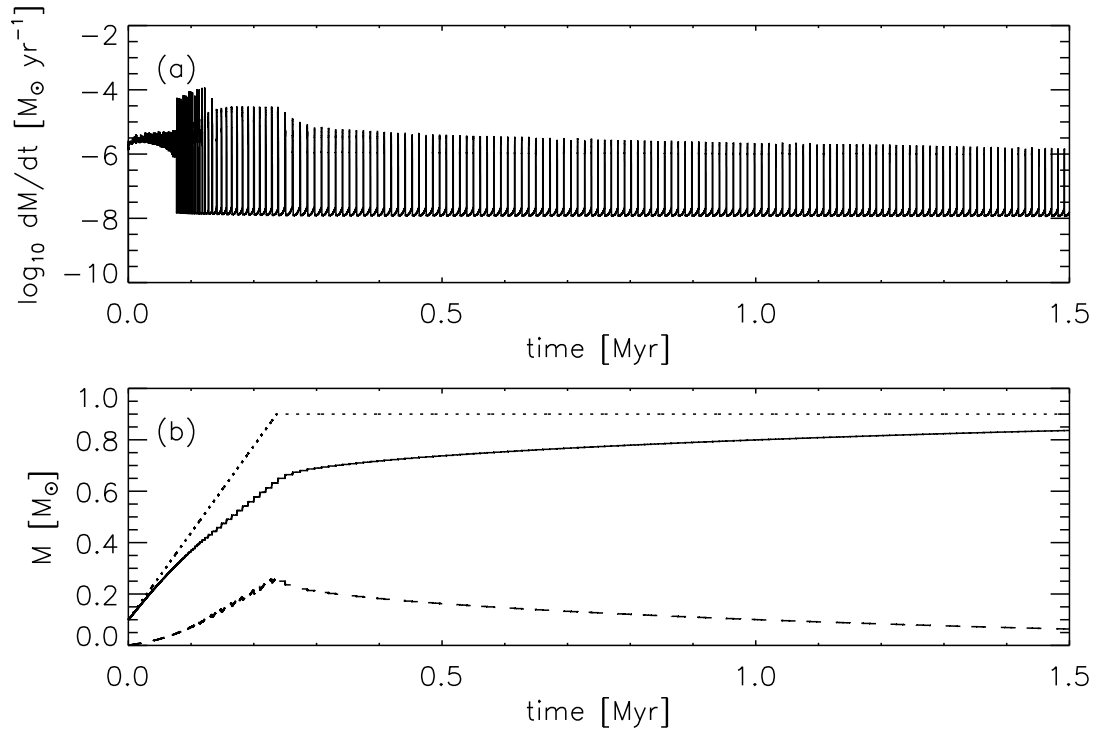


Fig. 6.— (a) Mass accretion rate and (b) mass of the central star + disk (dotted curve), mass of the central star (solid curve), and mass of the disk (dashed curve) with time for the standard non-zero DZRV model.

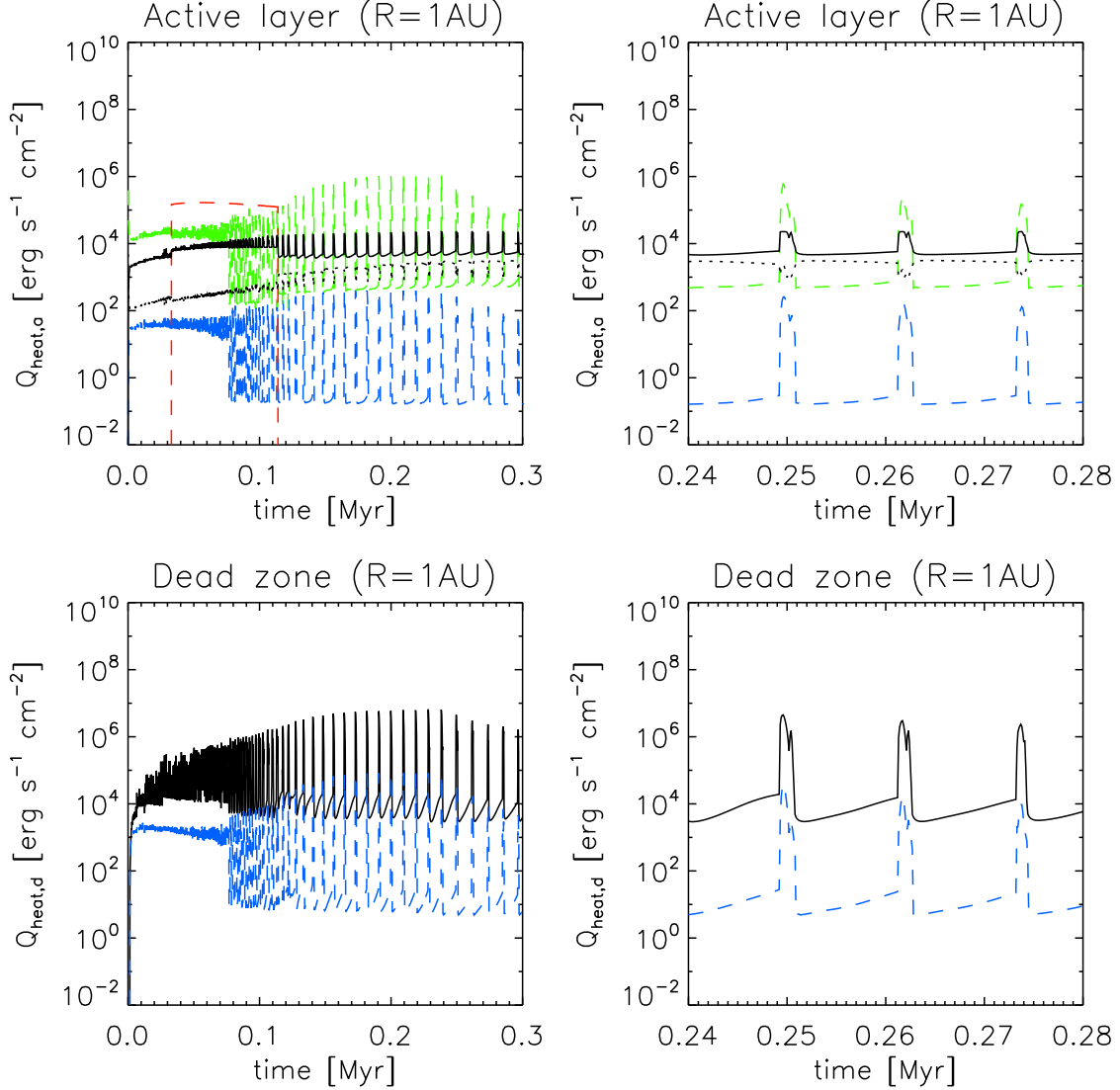


Fig. 7.— Various heating sources of the active layer (upper panels) and the dead zone (lower panels) at $R=1\text{ AU}$ for the first 0.3 Myr (left panels) and during a single outburst (right panels) with non-zero DZRV. Newly added heating sources in this paper are plotted in color while the heating sources have considered in (Zhu et al. 2010a,b) are presented with black curves. Upper panels: $Q_{\text{vis},a}$ (black solid), Q_* (black dotted), Q_{infall} (red dashed), Q_{acc} (green dashed), and $Q_{\text{grav},a}$ (blue dashed) are presented. Lower panels: $Q_{\text{vis},d}$ (black solid) and $Q_{\text{grav},d}$ (blue dashed) are presented.

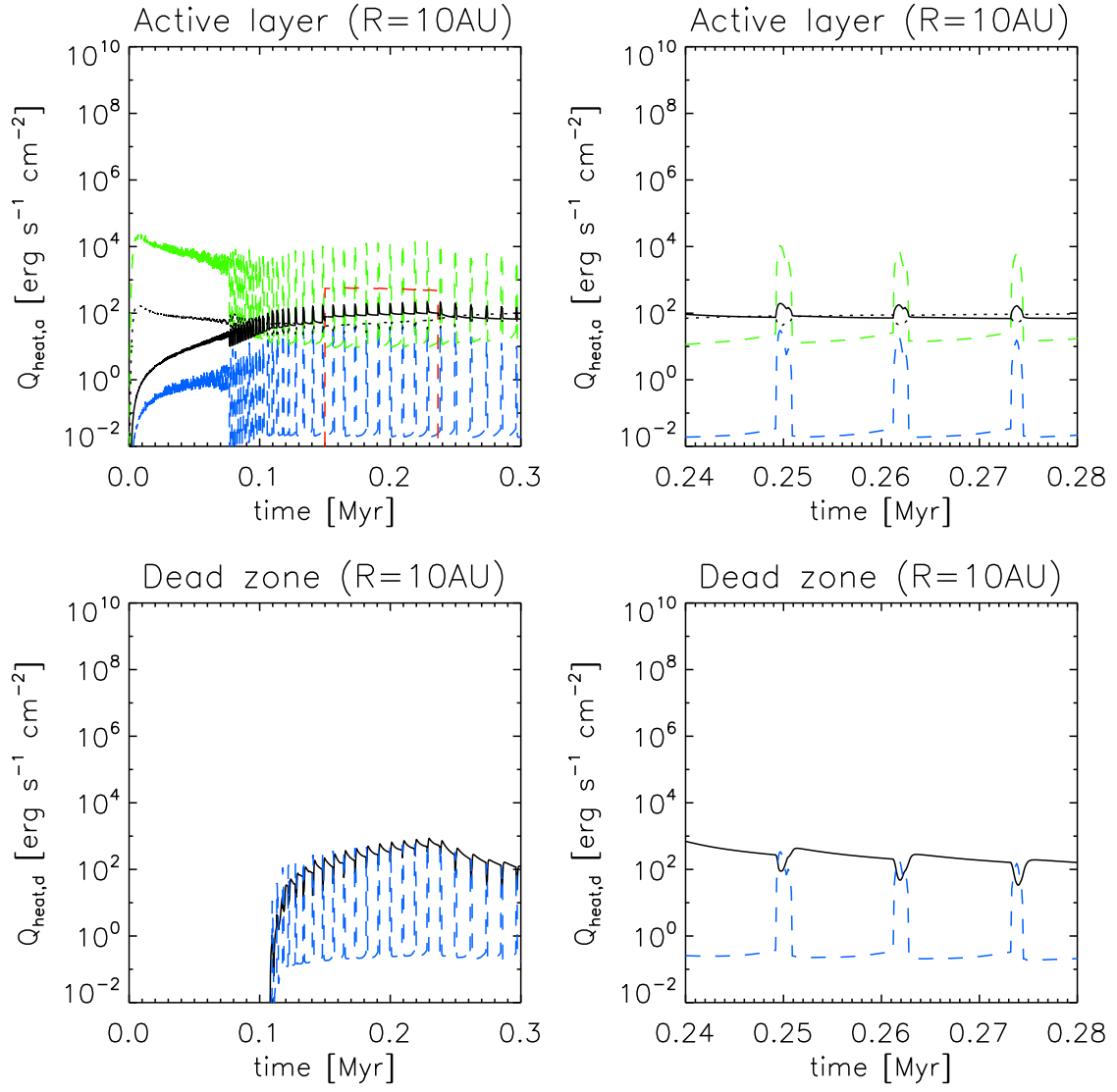


Fig. 8.— Same as Figure 7 but at $R = 10 \text{ AU}$.

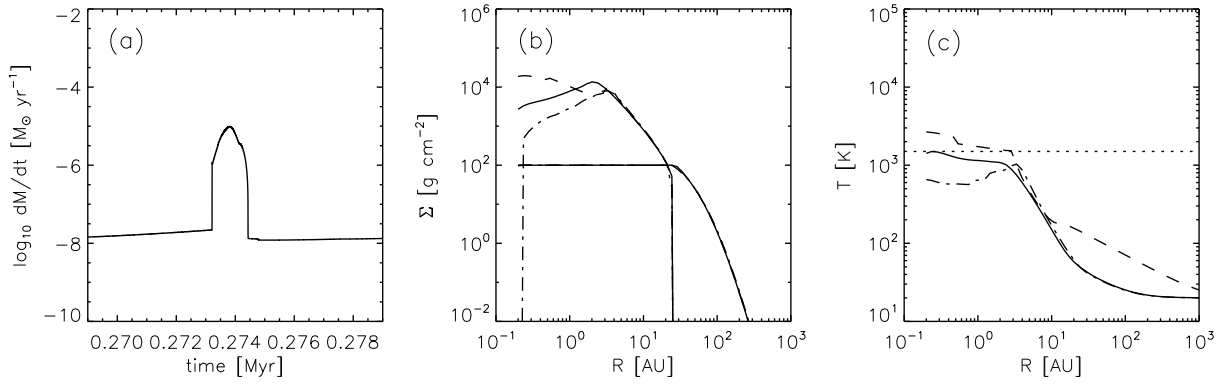


Fig. 9.— (a) Mass accretion rate of a single outburst of the standard non-zero DZRV model. Radial profiles of (b) the surface densities and (c) the midplane temperatures at the beginning (solid curves), at the maximum accretion rate (dashed curves), and at the end (dash-dotted curves) of the burst. In panel (b), the curves with higher surface densities at the inner disk represent the dead zone surface density while the lower ones extend further out represent the active layer. In panel (c), the dotted horizontal line represents the MRI activation temperature $T_{\text{MRI}} = 1500$ K.

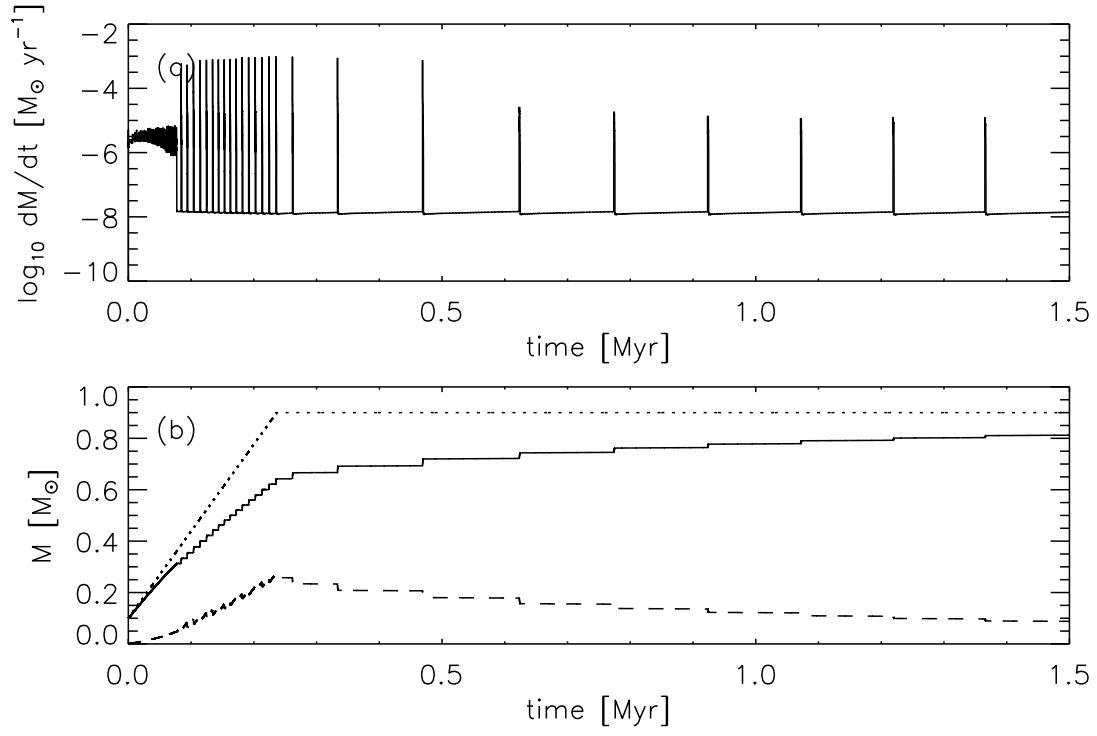


Fig. 10.— (a) Mass accretion rate and (b) mass of the central star + disk (dotted curve), mass of the central star (solid curve), and mass of the disk (dashed curve) of non-zero DZRV model as a function of time, with 10 % of accretion efficiency f_{rd} in the dead zone.

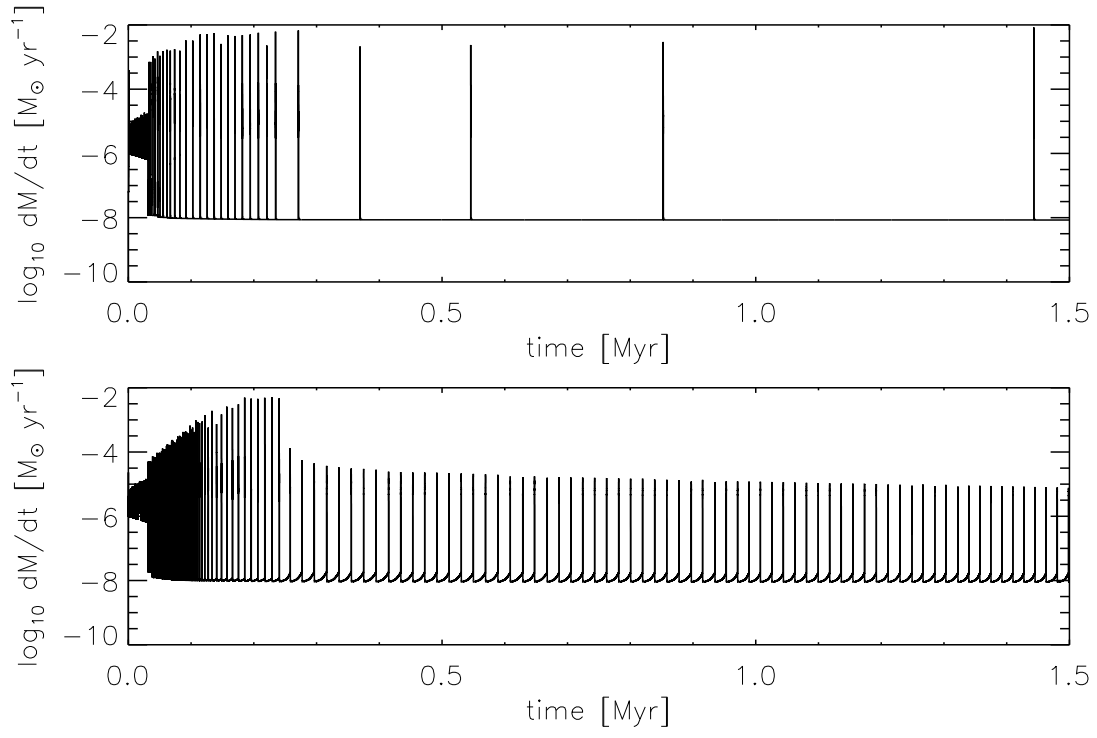


Fig. 11.— Mass accretion rate of zero DZRV model (upper) and non-zero DZRV model (lower) as a function of time, with $\Sigma_A = 20 \text{ g cm}^{-2}$ and $\alpha_{MRI} = 0.05$.

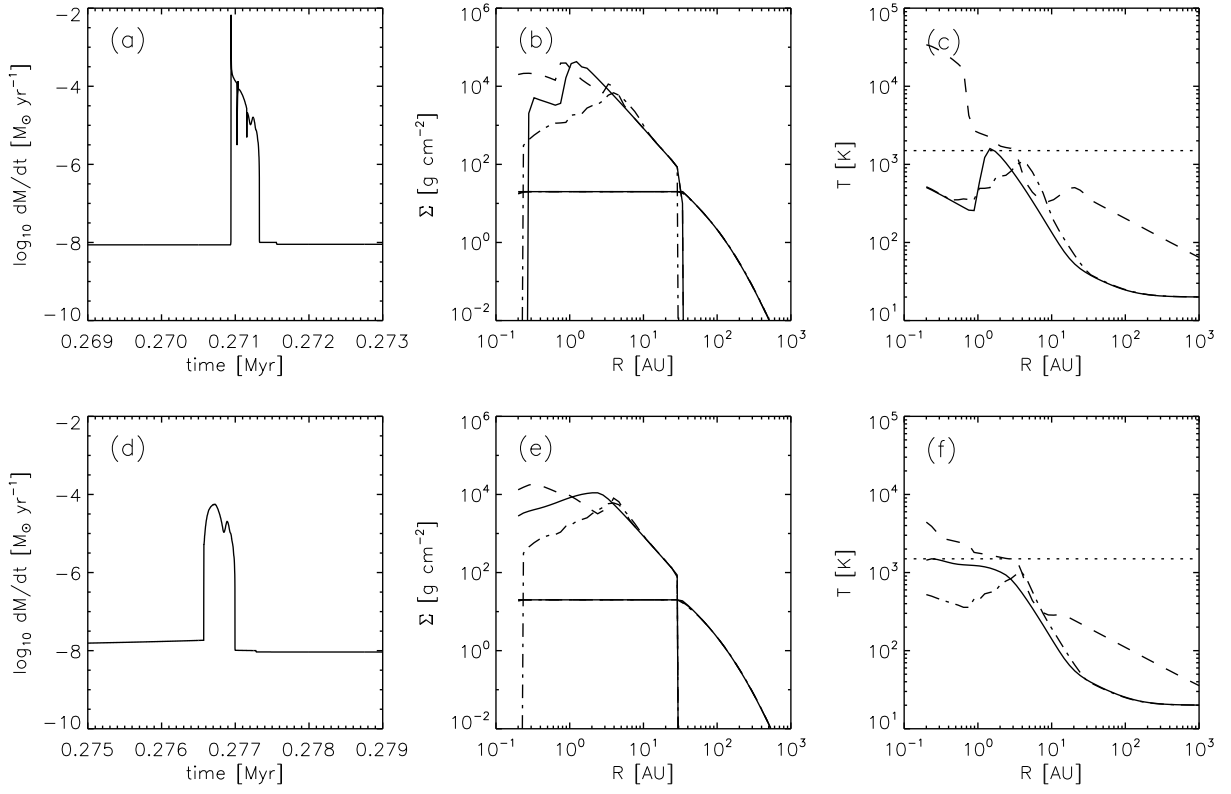


Fig. 12.— Same as Figure 5 (upper panels) and 9 (lower panels) but with $\Sigma_A = 20 \text{ g cm}^{-2}$ and $\alpha_{MRI} = 0.05$.

Table 1. Parameters and results

α_{rd}	α_{MRI}	Σ_A (g cm^{-2})	$R_{\text{dead}}^{\text{a}}$ (AU)	M_{*}^{a} (M_{\odot})	$M_{\text{disk}}^{\text{a}}$ (M_{\odot})	M_{in}^{a} (M_{\odot})	$M_{\text{out}}^{\text{a}}$ (M_{\odot})	$M_{\text{burst}}^{\text{b}}$ (M_{\odot})	$\dot{M}_{\text{max}}^{\text{b}}$ ($M_{\odot} \text{ yr}^{-1}$)	$\Delta t_{\text{burst}}^{\text{b}}$ (yr)	D_O^{c}	D_T^{d}
zero	0.01	100	29/5.5	0.64/0.76	0.26/0.14	0.21/0.08	0.05/0.06	0.027	1.11×10^{-3}	1340	0.06	0.005
non-zero	0.01	100	24/6.5	0.65/0.80	0.25/0.10	0.20/0.04	0.05/0.06	1.5×10^{-3}	3.17×10^{-6}	450	0.16	0.06
zero	0.05	20	33.9/7.6	0.65/0.80	0.25/0.10	0.22/0.08	0.03/0.02	0.028	4.34×10^{-3}	310	0.016	0.002
non-zero	0.05	20	33.9/7.6	0.65/0.82	0.25/0.08	0.22/0.05	0.04/0.03	4.6×10^{-3}	4.26×10^{-5}	200	0.08	0.015

^aQuantities are taken at 0.24 and 1 Myr.

^bOutburst quantities are averaged over time after infall ends.

^cDuty cycle during outburst stage.

^dDuty cycle during T Tauri phase.